

Algorithm Theoretical Basis for the Himawari-8, -9/AHI Cryosphere Product Part 2: Sea Ice Distribution

Yusuke IOKA*¹, Yusuke YOGO*², Tomonori TANIKAWA*³
Masahiro HOSAKA*⁴, Haruma ISHIDA*^{2, *5} and Teruo AOKI*^{6, *3}

Abstract

This paper describes the algorithm theoretical basis for the Himawari-8 and 9 Cryosphere Sea Ice Distribution product developed by JMA's Meteorological Satellite Center.

Single-scene sea ice distribution in the product is based on a decision tree method with static thresholds and computation combining a cloud detection algorithm and a sea ice detection algorithm in conjunction with a microwave sea ice product. The product incorporates a novel algorithm approach to produce one-day merged sea ice distribution results.

Validation of the product based on comparison with JMA's Northern Hemisphere Ice Distribution Chart showed consistency with related analysis. In the Sea of Okhotsk (135 – 152°E, 41 – 54°N), user's accuracy was approximately 0.9 – 1.0 and producer's accuracy was approximately 0.8 – 0.9 throughout winter. Sea ice boundary expressivity was also better than that of the Himawari-8 and 9 Cloud Mask Product. This sea ice information is expected to support coastal disaster prevention and safety in relation to marine traffic and tourism around the Sea of Okhotsk.

1. Introduction

Sea ice – a winter phenomenon caused by seawater freezing – floats on the ocean surface, enclosing polar and high-latitude ocean areas in ice pack conditions (Aota and Uematsu 1989).

Sea ice is a major characteristic of the Sea of Okhotsk and other parts of northern Japan, drifting from northern parts of this sea with wind and ocean currents and approaching the Hokkaido coast in winter (Aota 1974).

The phenomenon represents a valuable winter tourist resource and enriches ocean waters via plankton transport

(Kunimatsu et al. 1993). However, it can also seriously damage marine products and fishing facilities as well as obstructing shipping lanes, and occasionally causes ships to become stuck.

Sea ice forecasting based on numerical weather prediction (NWP) is important in consideration of climate change. Feedback based on the albedo contrast between water and sea ice is a key aspect of climate change monitoring, and helps to elucidate sea ice extents and thickness in areas of seasonal sea ice formation (Curry et al. 1995). Against such a background, the provision of accurate information on sea ice distribution and extent in

*¹ Satellite Application and Analysis Division, Data Processing Department, Meteorological Satellite Center (now at Shizuoka Local Meteorological Office, Japan Meteorological Agency)

*² Satellite Application and Analysis Division, Data Processing Department, Meteorological Satellite Center

*³ Department of Physical Meteorology, Meteorological Research Institute

*⁴ Department of Climate and Geochemistry Research, Meteorological Research Institute

*⁵ Department of Observation and Data Assimilation Research, Meteorological Research Institute

*⁶ National Institute of Polar Research

(Received 27 December 2018, Accepted 23 April 2019)

consideration of surface boundary conditions is important for sea ice forecasting in NWP.

Satellite observation supports the monitoring of sea ice distribution with a spatially and temporally high-resolution scale. Geostationary satellite observation is particularly useful in this area, enabling frequent observation of fixed regions. In this regard, satellite products allow the assimilation of satellite data in NWP on regional and global scales.

JMA’s latest Himawari-8 and 9 geostationary satellites carry Advanced Himawari Imager (AHI) featuring 16 bands in the visible, near-infrared and infrared regions (Bessho et al. 2016). Near-infrared bands are particularly useful for detecting snow and ice (Valovcin 1978, Aoki et al. 1999), and are used for this purpose in the Cloud Mask Product (CMP) (Imai and Yoshida 2016).

However, the implementation of sea ice detection as a subroutine in the CMP is associated with three issues in the sea ice product:

(1) The sea ice detection algorithm is based on the cloud mask technique of NWC-SAF for MSG/SEVIRI (Meteo-France 2016). This algorithm is utilized for SEVIRI imager processing, but the version used here was not suitable for the AHI imager even though both imagers have similar center wavelengths.

(2) The results of CMP sea ice detection are combined with the results of microwave sea ice detection based on OR conditions. This approach can be applied to identify sea ice through cloud cover, but with spatial/temporal resolution inferior to that of visible/infrared sea ice detection. Accordingly, the spatial resolution of the sea ice area is inferior to that of AHI data in areas of combined AHI and microwave sea ice detection.

(3) As the product is based on a four-day merged dataset by using OR conditions, sea ice area overestimation may adversely affect detection results over the four-day period. This dataset is also unable to accurately represent distribution changes relating to sea ice movement.

The sea ice detection algorithm was improved to resolve these issues. Although the spatial and temporal resolution of microwave satellite sensors (such as the Defense Meteorological Satellite Program special sensor

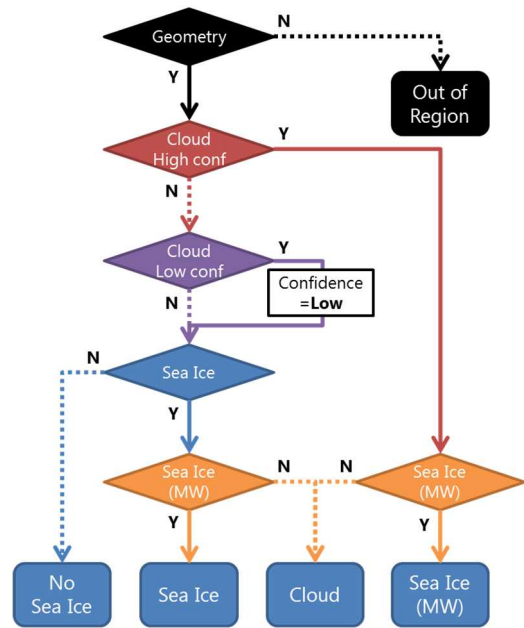


Fig. 1 Flow of the sea ice detection algorithm.

microwave imager (SSM/I) and the Advanced Microwave Scanning Radiometer 2 (AMSR2)) are inferior, the microwave data they provide can be applied to produce a reliable sea ice product. Accordingly, the sea ice product is formulated with microwave data for optimal accuracy based exclusively on the AHI sea ice product.

The improved sea ice detection algorithm is described in Section 2 below, results from the product are described in Section 3, validation is outlined in Section 4, an example of improved expression of sea ice boundaries is given in Section 5, and the paper is concluded and summarized in Section 6.

2. Algorithm

2.1 Overview

Figure 1 shows the process flow of the algorithm of sea/lake ice detection product. This product consists of cloud detection, cirrus detection and sea/lake ice detection. The algorithm of cloud detection is the same as that for the snow detection product (Yogo et al. 2019).

In the sea area, we use the microwave sea ice product as a supplemental data since microwave data provides reliable sea ice information under the cloud. Even in the clear sky area, it helps to detect the sea ice covered area.

Table 1 Specifications of AHI bands.

Band	Center wavelength [μm]	Spatial resolution at sub satellite point [km]
B01	0.47	1.0
B02	0.51	1.0
B03	0.64	0.5
B04	0.86	1.0
B05	1.6	2.0
B06	2.3	2.0
B07	3.9	2.0
B08	6.2	2.0
B09	6.9	2.0
B10	7.3	2.0
B11	8.6	2.0
B12	9.6	2.0
B13	10.4	2.0
B14	11.2	2.0
B15	12.4	2.0
B16	13.3	2.0

2.2 Input data

The inputs for the sea ice detection algorithm are Himawari Standard Data (HSD) and data from the microwave sea ice product.

AHI has 16 bands (B01 – B16) with varying spatial resolutions (Table 1). HSD full-disk data consist of 22,000 x 22,000 pixels for B03, 11,000 x 11,000 pixels for B01, B02 and B04, and 5,500 x 5,500 pixels for other bands (B05 – B16). The sea ice detection algorithm is applied to each infrared pixel (5,500 x 5,500).

The microwave sea ice product is derived by the Office of Marine Prediction at the Japan Meteorological Agency (JMA) using the NASA-Team algorithm (Swift and Cavalieri 1985) based on observation data from SSM/I and AMSR2.

2.3 Algorithm

In the algorithm, cloud detection part is same as that for the snow detection product from AHI (Yogo et al. 2019) to maintain continuity between land and ocean areas. The technical details of the cloud detection scheme are described in Yogo et al. (2019). The indices used in sea ice detection tests and microwave sea ice detection tests are described below.

2.3.1 Sea ice detection tests

Sea ice detection tests consist of three conditionals involving AND operators. If all the conditions are satisfied, the pixel is marked as clear sky over a sea ice surface:

$$NDSI = \frac{R_{0.51} - R_{1.6}}{R_{0.51} + R_{1.6}} > 0.4 \quad (1)$$

$$T_{10.4} < 272.15 [K] \quad (2)$$

$$R_{0.64} > 0.2. \quad (3)$$

Here, T_{λ} denotes the brightness temperature of the center wavelength λ , R_{λ} denotes the reflectance of the center wavelength λ , and NDSI denotes the normalized difference snow index. NDSI is based on the difference of reflectivity characteristics for snow and ice between the visible and short wave infrared bands.

As detailed analysis of numerous Landsat thematic mapper (TM) data for Sierra Nevada in California shows NDSI values of 0.4 corresponding to snow coverage of approximately 50% or more (Hall et al. 2016), this number was set as a threshold in the NDSI test. The second conditional application is used to clarify the characteristics of the part below the freezing area. The use of both visible and infrared band data increases sea ice pixel accuracy. The third conditional application is also used to increase sea ice pixel accuracy. In the visible band, reflectivity for sea ice is higher than for sea regions.

2.3.2 Microwave sea ice detection

The microwave sea ice product expresses total ice concentration (IC). In this test, $IC > 0$ is applied to define the sea ice area from the microwave sea ice product.

Microwave sea ice data are used in the Himawari-8/9 product to increase the accuracy of sea ice detection. Since the misclassification of ice cloud pixels as sea ice pixels affects the accuracy of sea ice detection, these data are applied at the post-sea ice detection stage to avoid the presentation of false sea ice pixels. The information also helps to clarify sea ice distribution under cloud cover, which is frequently observed during winter over the Sea of Okhotsk and hinders overall determination of sea ice areas from single Himawari-8/9 images. The use of data on microwave sea ice distribution as additional information on

cloud pixels helps to maximize the extent of sea ice distribution analysis. However, the spatial resolution of the microwave sea ice product from SSM/I or AMSR2 is 0.25° (approximately 25 km), which is lower than that of AHI data. In addition, the product has a one-day temporal resolution, and data from the previous day (or, if unavailable, from two or three days ago) are used. Thus, this is not a real-time dataset as opposed to the Himawari-8/9 product.

Against such a background, the microwave sea ice product is applied as a supplementary dataset in the Himawari-8/9 product.

3. Results

Figures 2 and 3 show the results of sea ice detection in the new product and the CMP product for 0300 UTC on February 8th 2016. The results obtained with the new product are largely consistent with those of the CMP product, but with clearer sea ice boundary characteristics (see Section 5 for details).

In the natural-color RGB composite imagery shown in Figure 4 (based on B05 (1.6 μm), B04 (0.86 μm) and B03 (0.64 μm) reflectance for the red, green and blue spectra, respectively) for 0300 UTC on February 8th 2016, snow and ice clouds are displayed in cyan because ice particles absorb the radiation in B05 (Lensky and Rosenfeld 2008).

In relation to Figures 2 and 3, the results of sea ice detection here are consistent with those from RGB composite imagery. Sea ice boundary expressivity is improved because the new product does not involve the use of an OR condition for merge with the microwave sea ice product.

Figure 5 shows the results of one-day sea ice product merge based on the algorithm used in the snow detection product (Yogo et al. 2019). The number of cloud pixels is reduced, and the clear-sky area is increased. As the Sea of Okhotsk is characterized by frequent winter cloud cover corresponding to the prevalent seasonal pressure pattern, the results of one-day merge can be expected to indicate a wider area of sea ice coverage than results from a single scene.

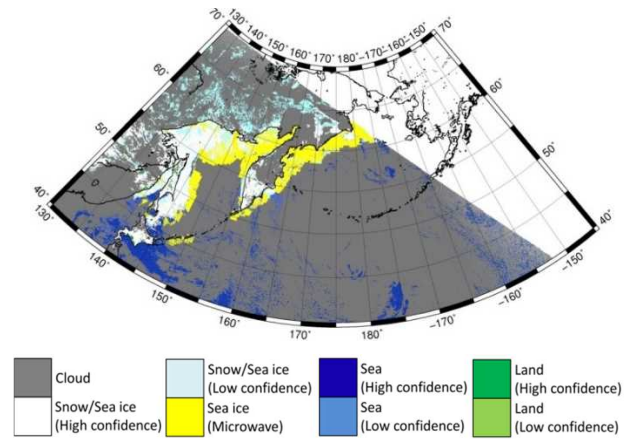


Fig. 2 Sea ice product, 0300 UTC, February 8th 2016. The white part in the upper right is outside the calculation area.

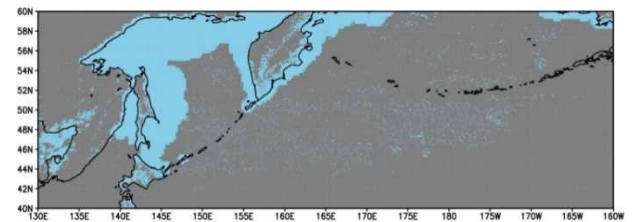


Fig. 3 CMP sea ice detection, 0300 UTC, February 8th 2016.

Light blue indicates areas of ice/snow coverage.

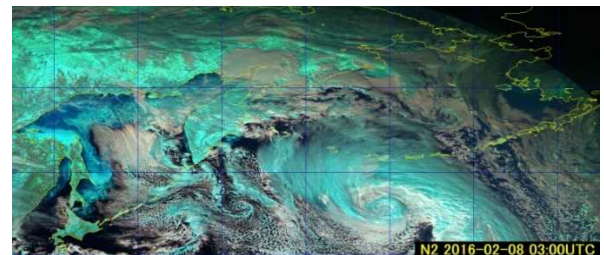


Fig. 4 Natural color RGB composite imagery, 0300 UTC, February 8th 2016.

Cyan indicates ice cloud, snow and sea ice.

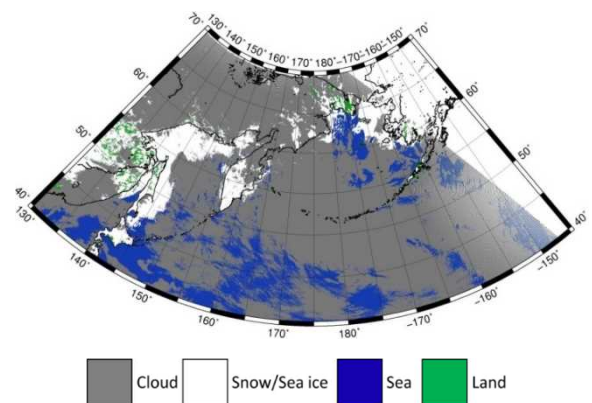


Fig. 5 Sea ice product merge, February 8th 2016.

4. Validation

The accuracy of the improved sea ice products was evaluated using a JMA Northern Hemisphere sea ice distribution chart, which is an analysis resource provided by the Agency’s Office of Marine Prediction based on the daily National Ice Center (NIC) ice boundary product from the Ice Mapping System (IMS) (Helfrich et al. 2007). For the Sea of Okhotsk, JMA manual analysis results are placed over NIC ice boundary product data in this application (see Table 2 for details).

In the study reported here, one-day merge results from the sea ice product for Tuesdays and Fridays were compared with the content of this chart, which is also provided on Tuesdays and Fridays only. To increase the content of datasets for validation, datasets from December to March of 2015/2016, 2016/2017 and 2017/2018 were used.

Overall accuracy (OA), producer’s accuracy (PA) and user’s accuracy (UA) were calculated as

$$OA = \frac{A + D}{A + B + C + D} ,$$

$$PA = \frac{A}{A + C} ,$$

$$UA = \frac{A}{A + B} ,$$

where A, B, C, D and E are the sample counts of elements based on comparison between the AHI sea ice product and sea ice charts as reference data, as defined in the error matrix of Table 3. OA is related to the general probability of a pixel being classified as sea ice and ocean, UA refers to the probability of a pixel classified as sea ice in the AHI actually being in this class, and PA refers to the probability of sea ice cover being classified as such. The difference between UA and PA is seen as a metric of under- or over-estimation in sea ice detection, with $UA > PA$ indicating underestimation and $UA < PA$ indicating overestimation.

Figure 6 shows validation results with a JMA Northern Hemisphere sea ice distribution chart for February 2016, 2017 and 2018, and Figure 7 shows the

Table 2 Northern Hemisphere sea ice distribution chart specifications.

Area	35 – 90°N, 180°W – 180°E
Spatial resolution	0.1 × 0.1°
Frequency	Every Tuesday and Friday

Table 3 Error matrix of sample counts for A, B, C, D and E. Rows show satellite-derived map categories, and columns show sea ice chart reference categories.

	Sea ice (chart)	Not sea ice (chart)
Sea ice (product)	A	B
Not sea ice (product)	C	D
Cloud	E	

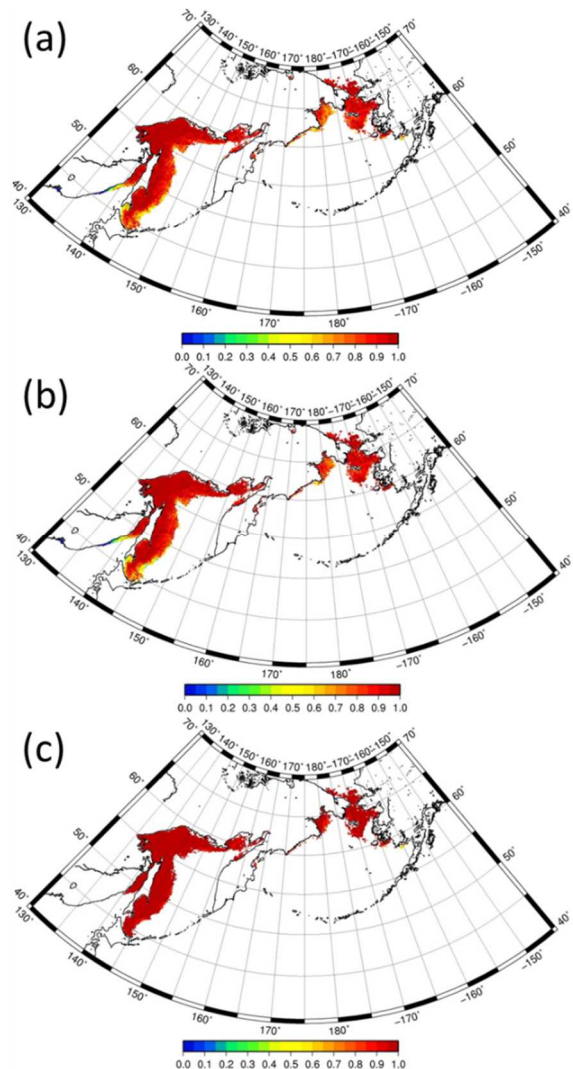


Fig. 6 Overall accuracy (a), producer’s accuracy (b) and user’s accuracy (c) with a Northern Hemisphere sea ice distribution chart for February.

same for the Sea of Okhotsk. High overall accuracy is seen for the validation area, but OA and PA exhibit relative decreases at the sea ice boundary.

One reason for this decrease relates to the characteristics of the sea ice boundary. The thinness of ice in this region makes it difficult to distinguish from ocean water in satellite imagery based on visible and near-infrared reflectivity.

Another reason relates to the superior spatial resolution of the sea ice detection product as compared to Northern Hemisphere sea ice distribution chart content, which can cause overestimation of sea ice presence in charts. This overestimation is reflected in validation results as a PA decrease if the results of sea ice detection are consistent with actual sea ice distribution.

The time-series representations of PA and UA accuracy in Figure 8 show generally high values (UA: approx. 0.9 – 1.0; PA: approx. 0.8) and only minor differences between the two, implying a slight underestimation of sea ice detection. This may be attributable to differences in spatial resolution between the AHI sea ice product and sea ice chart data.

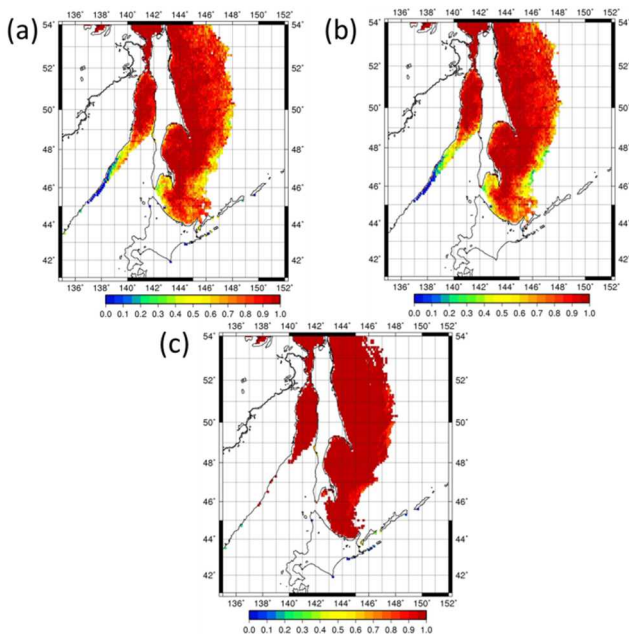


Fig. 7 Overall accuracy (a), producer's accuracy (b) and user's accuracy (c) with a Northern Hemisphere sea ice distribution chart for February in the Sea of Okhotsk.

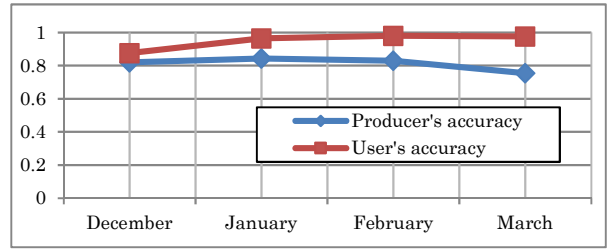


Fig. 8 Time-series representation of validation results with a Northern Hemisphere sea ice distribution chart for the Sea of Okhotsk (135 – 152°E, 41 – 54°N).

5. Improvement of sea ice boundary expressivity

Figure 9 shows natural color RGB imagery from the new product and the CMP product for 0300 UTC on February 8th 2016, with the former showing greater detail in sea ice conditions along coastal areas of Hokkaido, Aniva Bay and the Gulf of Patience. Such high-resolution sea ice information is especially useful for the Sea of Okhotsk. This is an advantage of AHI imagery over microwave product data.

As mentioned in the introduction, information on sea ice approaching the Hokkaido coast is important for continued operations relating to marine products, fisheries and shipping. Sea ice is also a valuable tourism resource in winter, and information on its approach is fruitful in this sector. Himawari-8/9 produces full-disk imagery every 10 minutes, thereby capturing the daily movement of sea ice.

In this way, such advanced sea ice information is useful in coastal disaster prevention, marine traffic safety and tourism around the Sea of Okhotsk.

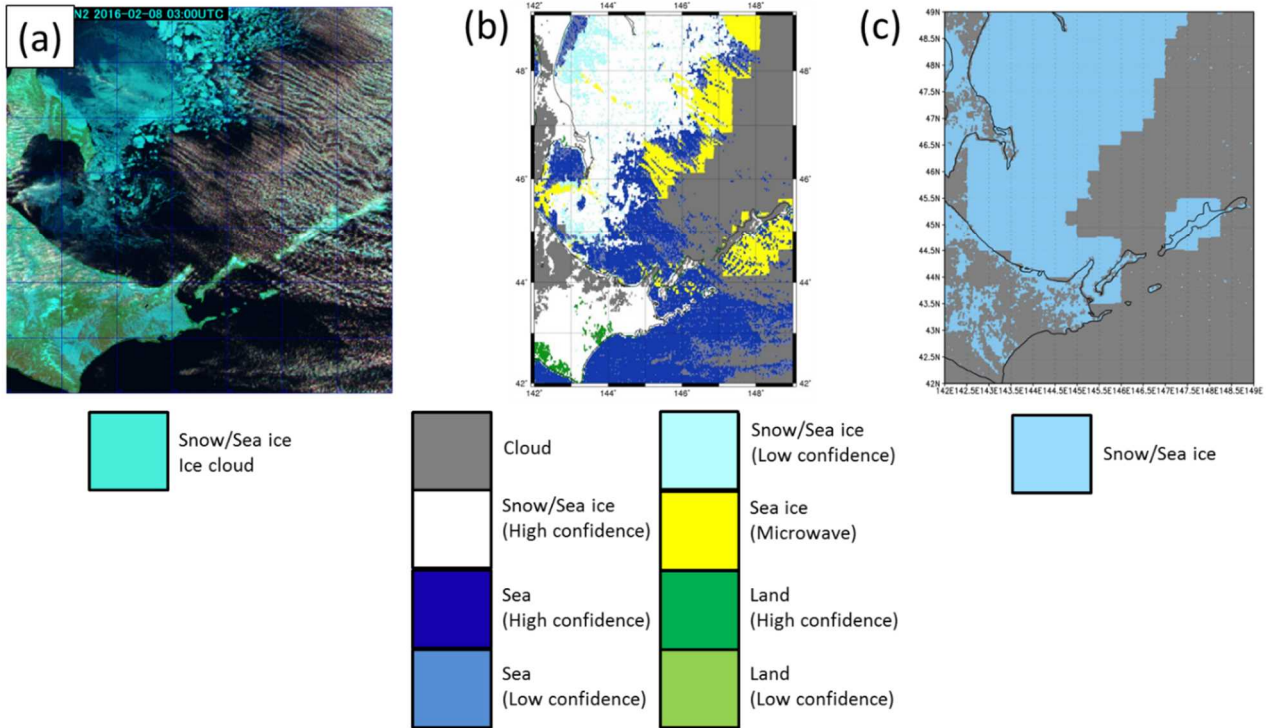


Fig. 9 Natural color RGB (a), sea ice detection (b) and CMP product sea ice detection (c) for 0300 UTC on February 8th 2016.

6. Summary

The research reported here was conducted to support the development of a new Himawari-8 and 9/AHI sea ice detection product.

The novel approach to single-scene sea ice detection is based on a decision tree method with a static threshold, and involves a cloud detection algorithm, a sea ice detection algorithm and combination with microwave sea ice product data. A one-day merged sea ice product was also developed by combining single-scene results with outcomes from the new algorithm (Yogo et al. 2019).

The consistency of single-scene results with RGB composite imagery is superior to that of RGB composite imagery alone. Spatial resolution at sea ice boundaries is improved via the new product's use of the new composite method with microwave sea ice product data. The product was verified with JMA Northern Hemisphere sea ice distribution data.

Statistical validation results (OA, PA, UA) showed that the new sea ice detection outcomes are consistent with analysis chart data and exhibit high accuracy for most of the

calculation area. Time-series representations of validation results show accuracy of approximately 0.9 – 1.0 for UA and approximately 0.8 for PA during the period from December to March.

These improved results are expected to contribute to improved cloud mask product data and subsequent level-2 products as well as supporting coastal disaster prevention and tourism.

References

- Aoki, Te., Ta. Aoki, M. Fukabori and A. Uchiyama, 1999: Numerical simulation of the atmospheric effects on snow albedo with a multiple scattering radiative transfer model for the atmosphere-snow system. *J. Meteor. Soc. Japan*, **77**, doi: 10.2151/jmsj1965.77.2_595
- Aota, M., 1974: On the Drift Ice of the Sea of Okhotsk. *The Quaternary Research*, **12**, 235-240, doi: 10.4116/jaqua.12.235
- Aota, M. and E. Uematsu, 1989: The Study on the Polar Ocean and the Sea of Okhotsk. *Journal of Geography*,

98, 600-612, doi: 10.5026/jgeography.98.5_600

- Bessho, K., K. Date, M. Hayashi, A. Ikeda, T. Imai, H. Inoue, Y. Kumagai, T. Miyakawa, H. Murata, T. Ohno, A. Okuyama, R. Oyama, Y. Sasaki, Y. Shimazu, K. Shimoji, Y. Sumida, M. Suzuki, H. Taniguchi, H. Tsuchiyama, D. Uesawa, H. Yokota, and R. Yoshida, 2016: An introduction to Himawari-8/9 - Japan's new-generation geostationary meteorological satellites. *J. Meteor. Soc. Japan*, **94**, doi:10.2151/jmsj.2016-009.
- Curry, J. A., J. L. Schramm and E. E. Ebert, 1995: Sea Ice-Albedo Climate Feedback Mechanism. *Journal of climate*, **8**, 240-247, doi:10.1175/1520-0442(1995)008<0240:SIACFM>2.0.CO;2
- Hall, D. K. and G. A. Riggs, 2016: MODIS/Terra Snow Cover 5-Min L2 Swath 500 m, Version 6. *Boulder, Colorado USA. NASA National Snow and Ice Data Center Distributed Active Archive Center.*
doi: 10.5067/MODIS/MOD10_L2.006
- Helfrich, S. R., D. McNamara, B. H. Ramsay, T. Baldwin, and T. Kasheta, 2007: Enhancement to, and forthcoming developments in the Interactive Multisensor Snow and Ice Mapping System (IMS). *Hydrol. Processes*, **21**, 1576-1586, doi:10.1002/hyp.6720.
- Imai, T. and R. Yoshida, 2016: Algorithm Theoretical Basis for Himawari-8 Cloud Mask Product. *Meteorological Satellite Center Technical Note*, **61**, 1-16.
- Kunimatsu, S., F. Hara., Y. Takahashi., H. Saeki., K. Enoki. and A. Imaizumi., 1993: Study on size of drift ice at the Okhotsk Sea Coast of Hokkaido. *PROCEEDINGS OF CIVIL ENGINEERING IN THE OCEAN*, **9**, 95-100, doi:10.2208/prooe.9.95
- Lensky, M. and D. Rosenfeld, 2008: "Clouds-Aerosols-Precipitation Satellite Analysis Tool(CAPSAT)", *Atmos. Chem. Phys.*, **9**, 6739-6753.
- Meteo-France, 2016: Algorithm Theoretical Basis Document for the Cloud Product Processors of the NWC/GEO. Available at http://www.nwcsaf.org/documents/20182/30662/NWC-CDOP2-GEO-MFL-SCI-ATBD-Cloud_v1.1.pdf/a5bb6eca-871b-4707-9c76-e0be09915d94
- Swift, T. C and J. D. Cavalieri, 1985: Passive Microwave Remote Sensing for Sea Ice Research, *Eos, Transactions American Geophysical Union*, **66**, 1210-1212.
doi: 10.1029/EO066i049p01210|
- Valovcin, F. R., 1978: Spectral radiance of snow and clouds in the near infrared spectral region. *Air Force Geophysics Laboratory, Hanscom, MA*, AFGL-TR-78-0289
- Yogo, Y., Y. Ioka, T. Tanikawa, M. Hosaka, H. Ishida and T. Aoki, 2019: Algorithm Theoretical Basis for the Himawari-8, -9/AHI Cryosphere Product Part 1: Snow Cover. *Meteorological Satellite Center Technical Note*, **64**, 1-12.

ひまわり 8・9号による雪氷域検出プロダクト その2：海氷域

井岡佑介*1、余郷友祐*2、谷川朋範*3、保坂征宏*4、石田春磨*2, *5、青木輝夫*6, *3

要旨

気象庁が運用する新世代静止気象衛星ひまわり 8・9号は、従来の衛星よりも時間解像度、空間解像度、そして波長帯の数を改良した可視赤外放射計 Advanced Himawari Imager (AHI)を搭載している。気象衛星センターでは、これらの観測性能の向上で追加された観測波長帯を用いた新条件式や、高頻度観測を活用した複数シーン結合処理を導入した海氷域検出プロダクトの開発を行った。このプロダクトでは、決定木法による単一シーンの海氷検出を、ひまわりの観測画像とマイクロ波衛星を用いた海氷プロダクトを使用して行い、それを一日分合成することで、単一シーンの検出と比較して海氷域の検出域を向上させている。

2016年、2017年、2018年の冬季について気象庁の海氷解析図である北半球海氷分布図との比較を行ったところ、オホーツク海(135 – 152°E, 41 – 54°N)において空振りの少なさと対応する user's accuracy は 0.9 から 1.0、見逃しの少なさと対応する producer's accuracy は 0.8 から 0.9 となり、高い精度で海氷域を検出できていることがわかった。また、既存の雲マスクプロダクトにおいて行われている海氷検出サブルーチンと比較して、マイクロ波衛星の海氷データを使用するアルゴリズムの改良によって海氷縁辺部の表現性が向上したことも示された。

*1 気象衛星センターデータ処理部解析課 (現：気象庁静岡地方气象台)

*2 気象衛星センターデータ処理部解析課

*3 気象研究所気象予報研究部

*4 気象研究所気候・環境研究部

*5 気象研究所気象観測研究部

*6 国立極地研究所

(2018年12月27日受領、2019年4月23日受理)